FORTIFIKATORISK

NOTAT NR. 83 / 72

UNDERGROUND AMMUNITION STORAGE

Blast Propagation in the Tunnel System

Report V A

CONNECTED CHAMBER STORAGE
BLAST LOAD ON DOORS IN THREE SITES

FORSVARETS BYGNINGSTJENESTE

NORWEGIAN DEFENCE CONSTRUCTION SERVICE
Office of Test and Development

(14) Fortifikatorisk notat nr 83/72

(6) UNDERGROUND AMMUNITION STORAGE.
Blast Propagation in the Tunnel System.

Report V A.

CONNECTED CHAMBER STORAGE
BLAST LOAD ON DOORS IN THREE SITES.

by

(10) A. T. Skjeltorp, T. Hegdahl and A. Jenssen

(11) Sep 75

(12) 32 p.

September 1975

403634

NORWEGIAN DEFENCE CONSTRUCTION SERVICE
Office of Test and Development

Fortifikatorisk notat nr 83/72

UNDERGROUND AMMUNITION STORAGE

Blast Propagation in the Tunnel System

Report V A

CONNECTED CHAMBER STORAGE
BLAST LOAD ON DOORS IN THREE SITES

by

A.T. Skjeltorp, T. Hegdahl, and A. Jenssen

September 1975

T A B L E O F C O N T E N T S

A B S T R A C T

This report reviews the result from airblast measurements in models of three particular types of underground ammunition storage sites. The use of simple scaling relationship are shown to reproduce the blast data reasonably well for a wide range of geometrical parameters. One of the models is geometrically similar to a large scale test site in rock and direct comparison of the model and full scale data shows the blast reducing effects of wall roughness.

1. INTRODUCTION

This report is the fifth in a series of five /1-5/* describing the results from an extensive series of model tests on the blast effects in underground ammunition storage sites in case of accidental explosions. In the preceeding reports details were given of the test programme /1/ and measurements were reported of chamber pressure /2/, airblast in the tunnel system of single chamber storage sites /3/, and connected chamber storage sites /4/. In the present report, data are presented on the air blast in three particular types of storage sites, one of which has been tested in large scale. In particular, direct comparison between the model and full scale data will show the importance of large wall roughness attenuation in the tunnel system blasted out of rock.

The basic scaling relationship employed in the present work are reviewed briefly in Sec. 2, followed by a short presentation of the experimental details in Sec. 3. The experimental results are analysed in Sec. 4, and the principal results are finally summarized in Sec. 5.

2. THEORETICAL CONSIDERATIONS

2.1 Scaling Relationships

As for the preceeding reports, the basis for the proposed scaling relationship in the present report is the familiar Hopkinson's scaling laws /6/, which were reviewed in Report I /1/. To analyse the present data, the scaling relationships proposed in Report IV /4/, will be employed. In the analysis of the data in Sec. 4, direct reference will be made to these earlier results.

---

* Numerals inside slashes refer to appended references.

2.2 Non-Scaling Energy Losses

As was discussed in Report I /1/, the simple Hopkinson's scaling laws do not account for energy dissipating effects to the walls, of which only the viscous loss due to wall roughness is expected to be significant. This effect is being dealt with by using a model originally proposed by Porzel /7/, which was reviewed in Report I /1/. However, for the relatively smooth-walled steel tubes used in the present tests, the effects of wall roughness is expected to be relatively small. This will be discussed in more detail in Sec. 4, and in particular the analysis of the results from a large scale test will clearly demonstrate the importance of wall roughness.

3. EXPERIMENTAL DETAILS

Details of models, instrumentation, and data reduction are to be found in Report I /1/, and we shall therefore only summarize the main features here.

3.1 Models

Fig. 3.1a shows the three models, Model 1, 2, and 3 used in the tests. Model 1 represents a situation with only one exit. The length of the dead end tunnel was L/D = 7 and 29 as expressed in tunnel diameters, and the blast was measured at various positions in the main passage-way as well as at the dead end. This model is similar to one of the models with two exits discussed in Report IV.

Model 2 in Fig. 3.1a is almost geometrically similar to a large scale test site at Raufoss /8/ shown in Fig. 3.1b. The linear scaling factor between the model and prototype was n = 19,7.

There were, however, some differences between the model and prototype: (1) cylindrical storage chamber and tunnels in the model compared to semi-cylindrical ones in the prototype; (2) a small bend (20^{o}) in the prototype tunnel, and (4) significant wall

roughness in the prototype tunnel blasted out of rock compared to an essentially insignificant wall roughness in the steel tubes of the model. Of these only (3) is expected to produce significantly different blast propagation in the tunnel system. This will be analysed more detailed in Sec. 4.

Model 3 represents a situation where the branch passageways leading into adjacent chambers are closed with blast-proof doors to prevent detonation propagation from one storage chamber to the next. For this model, the blast was measured in the tunnel system as well as at the positions of the doors.

3.2 Explosive

The pressed TNT charges used in the tests were suspended in the middle of the detonation chamber and initiated with electrical blasting cap no 8. This has an equivalent TNT weight of $1,5 \pm 0,5$ g.

3.3 Instrumentation and Data Reduction

To measure the pressure-time history in the models, standard measurement techniques were used and the blast wave parameters were evaluated employing special computer programmes. The total incertainty in the peak pressure was estimated to be about 10%, whereas the uncertainty in the impulse was estimated to be about 30%. For further details, reference is made to Report I /1/.

4. EXPERIMENTAL RESULTS AND ANALYSIS

Only the most significant results will be presented in the following sections as part B of this report, Report V B, contains all the pressure-time recordings and tabulations of blast wave parameter values.

4.1 Peak Pressure Data Model 1 and 2

Because of the dead end tunnel in these models (Fig. 3.1a), the pressure-time recordings

showed certain pecularities which are exemplified in Figs. 4.1a - 4.1c as smooth curve reproductions. The most pronounced features here are the appearences of two or more peaks: One caused by the direct blast wave, and the others by the superposition of the direct blast and the reflected blast from the dead end wall. As indicated, the peak pressures are defined as being the maximum pressures regardless of whether this originates from the direct blast or the superimposed blast.

Refering to Report IV /4/, the peak pressure data in the tunnel of a connected chamber storage site with two exits appeared to scale according to

$$p = C_1(Qx_{\pm}/V_t)^{C_2} \qquad (4.1a)$$

with

Q = explosive charge weight

V_t = combined volume of storage chamber, branch passage-way, and main passage-way up to the observation point

$x_{\pm}$ = energy distribution factor

C_1 = scaling coefficient

C_2 = scaling exponent

These earlier results are now extended to the dead-end tunnel system of Model 1 and Figs. 4.1d and 4.1e show the definitions of terms used in Eq. (4.1a) for $L < L_D$ and $L > L_D$, respectively. Here L_D is the length of dead-end tunnel.

Fig 4.1f shows the peak pressure data p_+ (towards the exit) versus Qx_+/V_t. As may be seen, the data appear to fall on one universal curve. To test this hypothesis, least squares fits of Eq. (4.1a) were made to the three sets of data. This produced the following results:

Model 1, $L_D/D = 7,5$:

$$p_+ = (11 \pm 2)\ (Qx_+/V_t)^{0,37 \pm 0,05} \qquad (4.1b)$$

Model 1, $L_D/D = 29$:

$$p_+ = (10 \pm 3)\ (Qx_+/V_t)^{0,31 \pm 0,07} \qquad (4.1c)$$

Model 2, $L_D/D = 4,2$:

$$p_+ = (8,1 \pm 1,0)\ (Qx_+/V_t)^{0,37 \pm 0,02} \qquad (4.1d)$$

Thus, within the stated error limits, the data appear to be consisted with the universality hypothesis. An extended fit combining all the data produced the following result:

$$p_+ = (8 \pm 1)\ (Qx_+/V_t)^{0,42 \pm 0,05} \qquad (4.1e)$$

4.2 Comparison Model 2 and Prototype Data

As discussed earlier (Sec. 3.1), Model 2 was geometrically similar to a large scale test site in rock /8/. In Figs. 4.2a - 4.2c direct comparisons are made between the model and prototype peak pressure data. As the prototype data were obtained from shock front velocity measurements /8/, two sets of data are given for the model: one set found directly from the pressure-time recordings (open circles) and one set also found from shock front velocity measurements. As may be seen, these two techniques produce approcimately the same results.

However, the prototype data are much lower than the model data. This is to be expected due to the much larger wall roughness in the prototype. To see the possible effects of this wall

roughness, the prototype data were analysed using the model discussed in Report III:

$$p_o = C_1(Q/V_t)^{C_2} \qquad (4.2a)$$

$$Y(p_o) - Y(p) = (C_3/D)(L/D) \qquad (4.2b)$$

where:

p_o = fictitious peak pressure without wall friction

p = measured peak pressure

$Y(p_o)$ = impedanse function of p_o [Eq.(2.3b),Report II

$Y(p)$ = impedance function of p [Eq.(2.3b),Report II

C_1 = scaling factor

C_2 = scaling exponent

C_3 = $2\xi\,\bar{e}$ = effective wall roughness, see Report I

A nonlinear least squares fit of Eqs.(4.2a) and (4.2b) to the prototype data produced

$$p_o = (3{,}8 \pm 1{,}3)(Q/V_t)^{0{,}46 \pm 0{,}05} \qquad (4.2c)$$

$$C_3 = 0{,}17 \pm 0{,}03 \text{ m} \qquad (4.2d)$$

This fit reproduced the data within an average scatter of approximately 15%.

It may be noted that the numerical value for the effective wall roughness, $C_3 = 2\epsilon\,\bar{e}$, is quite consistent with direct observations /9/.

It is possible to extract the experimental "smooth-walled" data from Eq. (4.2b), and the results are shown in Fig. 4.2d. This figure also includes the model data.
As may be seen, the prototype data are consitently lower than the model data. It has not been possible

to account for this dicrepancy, but there are two factors which may have constributed: (1) the presence of relatively large amounts of dust and water in the prototype installation, and (2) the use of quite old and loosely packed TNT charges. In regard to (1), Swedish model tests have shown that the blast may be reduced significantly when the explosive charge is in close contact with relatively large amount of water (comparable to the explosive weight) /10/. However, rough estimates indicate that this effect alone will not account for the discrepancy. As for (2), the TNT used was many years old and could well have been less efficient than ordinary TNT. Besides, the total charge was made up of relatively loosely packed TNT-filled cartridges. Unfortunately, no free-field calibration tests were performed, and it is therefore not possible to be more specific at this point.

4.3 Impulse and Positive Duration for Model 1 and 2

As usual, the results for impuls and positive duration are more difficult to combine empirically than those for the front pressure. However, an attempt will be made to analyse the data according to the proposed scaling relationships in Report IV /4/ for a connected chamber storage with two exits:

$$IA_k/Q = D_1(Qx_+/V_t)^{D_2}\exp(-F_3L/D) \qquad (4.3a)$$

$$t_+A_k/Q = E_1(Qx_+/V_t)^{E_2}\exp(-E_3L/D) \qquad (4.3b)$$

Figs. 4.1d and 4.1e show the definitions of the terms used in these equations.

Following this scheme, Figs. 4.3a and 4.3b show the scaled impulse and positive duration data versus effective loading density. As a first approximation, the results appear to fall on discrete curves with the proposed empirical functional dependence.

Non-linear least squares fits of all the data to eqs.(4.3a) and (4.3b) produced the following results:

$$IA_k/Q = (50\pm2)(Qx_+/V_t)^{(-0,61\pm0,05)}\exp(-0,05\pm0,01)L/D \quad (4.3c)$$

$$t_+A_k/Q = (27\pm1)(Qx_+/V_t)^{(-0,97\pm0,08)}\exp(-0,07\pm0,01)L/D \quad (4.3d)$$

This appear to be quite satisfactory considering the large uncertainties involved in the interpretation of these quantities.

4.4 Results - Model 3

Fig. 4.4a shows typical smoothed reproductions of the pressure-time recordings in Model 3 (Fig. 3.1a). The most pronounced features here are the appearences of rounded peaks, which are due to the complicated diffraction patterns in this model. As for the other models, the peak pressures are defined as the maximum pressures and which not necessarity are the front pressures.

Table 4.4 shows the peak pressures and positive durations at the dead end walls in the branch passage-way (i.e. the positions where blast doors would be situated). These results are of course only valid for exactly geometrically similar full scale installations.

It may be noted that the peak pressures at MP 2 are only approximately half the valves at MP 1. Furthermore, for the highest loading density of 50 kg/m^3, the pressures are below 100 bar at MP 1 for all the configurations tested. This would imply that 100 bar doors will be sufficient for the prevention of detonation propagation from one chamber to adjacent chambers.

Measurements in the passageway were made out to approximately L/D = 55, from the chamber exit with loading densities Q/V_i = 25 - 50 kg/m^3 for the four combinations of V_i and L_1', shown in Fig. 3.1a. Fig. 4.4b shows the peak pressures versus an effective loading density Qx_+/V_t as defined earlier. The data were apparently relatively insensitive to V_i and L_1', and no distinction are made in the figure. However, the data appeared to fall on two curves p_+ and p_- as shown. Least squares fits produced

$$p_+ = 2{,}7(Qx_+/V_t)^{0{,}8} \qquad (4.4a)$$

and

$$p_- = 3{,}4(Qx_-/V_t)^{0{,}6} . \qquad (4.4b)$$

In the region of overlap $p_- < p_+$, which seems to indicate that the branch passage-way on the negative side acted as an efficient blast trap. However, due to the limited range of observations it is hardly possible to be more specific.

5. SUMMARY AND CONCLUSIONS

The methods developed in this report for the prediction of blast wave propagation in three special models may prove useful in the planning of full scale installations in rock.

The results provide a simple and sufficiently accurate method for the determination of the blast wave parameters at any point in the transport tunnel for a wide range of loading densities and geometries.

Direct comparisons of the present results have been made with one large scale test with a similar tunnel system, but with a much larger relative wall roughness. The relatively large difference in the peak

pressure attenuation for the model and large scale tests, has been partly accounted for as being due to the difference in wall roughness, but there are other effects in the full scale case which are not well understood.

REFERENCES

1. A. Skjeltorp, T. Hegdahl, and A. Jenssen, "Underground Ammunition Storage I: Test Program, instrumentation and data reduction". Technical note no 80/72, Norwegian Defence Construction Service (1975).

2. A. Skjeltorp, T. Hegdahl, and A. Jenssen, "Underground Ammunition Storage II A and II B: Chamber Pressure", Technical note no 79/72, Norwegian Defence Construction Service (1975).

3. A. Skjeltorp, T. Hegdahl, and A. Jenssen, "Underground Ammunition Storage III A and III B: Singel chamber storage. Variable tunnel diameter and variable chamber volume", Technical note no 81/72, Norwegian Defence Construction Service (1975).

4. A. Skjeltorp, T. Hegdahl, and A. Jenssen "Underground Ammunition Storage IV A and IV B: Connected chamber storage with variable chamber volume and variable angle between branch and main passageway". Technical note no 82/72, Norwegian Defence Construction Servide (1975).

5. The reports in Refs 2-4 labeled A contain the main results whereas the reports labeled B contain the raw data in the form of pressure-time recordings and tabulated blast wave parameters.

6. See for example W.E. Baker, P.S. Westine, and F.T. Dodge, "Similarity Methods in Engineering Dynamics" (Hyden Book Co., New Jersey, U.S.A., 1973) Ch. 4.

7. F.B. Porzel, "Study of Shock Impedance Effects in a Rough Walled Tunnel", Research Paper No. P-330, Institute for Defence Analysis (1969) (AD 684790).

8. K.G. Schmidt, "Underground Explosion Trials at Raufoss 1968: Blast Wave Propagation Following a Detonation in a Tunnel System", Norwegian Defence Research Establishment, Report no. X-128 (1970).

9. A.T. Skjeltorp, "Airblast Propagation Through Tunnels and the Effects of Wall Roughness", Technical note no. 103/75, Norwegian Defence Construction Service (1975).

10. S. Eriksson, "Water in Explosive Storage", 4th International Symposium on Military Applications of Blast Simulations, AWRE, Foulness, England, (1974), paper F 1.

Table 4.4. Blast data at measuring points MP1 and MP2 in Model 3 for various test configuration, see Fig. 3.1a.

Chamber volume V_i (cm^3)	Length L'_1 (cm)	Loading density Q/V_i (kg/m^3)	Measuring point	Average peak pressure p(bar)	Pos. duration t_+ (ms)
12150	20	25	MP 1	50	40
12150	20	25	MP 2	26	50
12150	20	50	MP 1	75	37
12150	20	50	MP 2	38	43
12150	30	25	MP 1	47	50
12150	30	25	MP 2	26	40
12150	30	50	MP 1	82	70
12150	30	50	MP 2	45	60
18500	20	25	MP 1	50	50
18500	20	25	MP 2	27	50
18500	20	50	MP 1	90	55
18500	20	50	MP 2	45	60
18500	30	25	MP 1	55	50
18500	30	25	MP 2	29	55
18500	30	50	MP 1	95	45
18500	30	50	MP 2	55	60

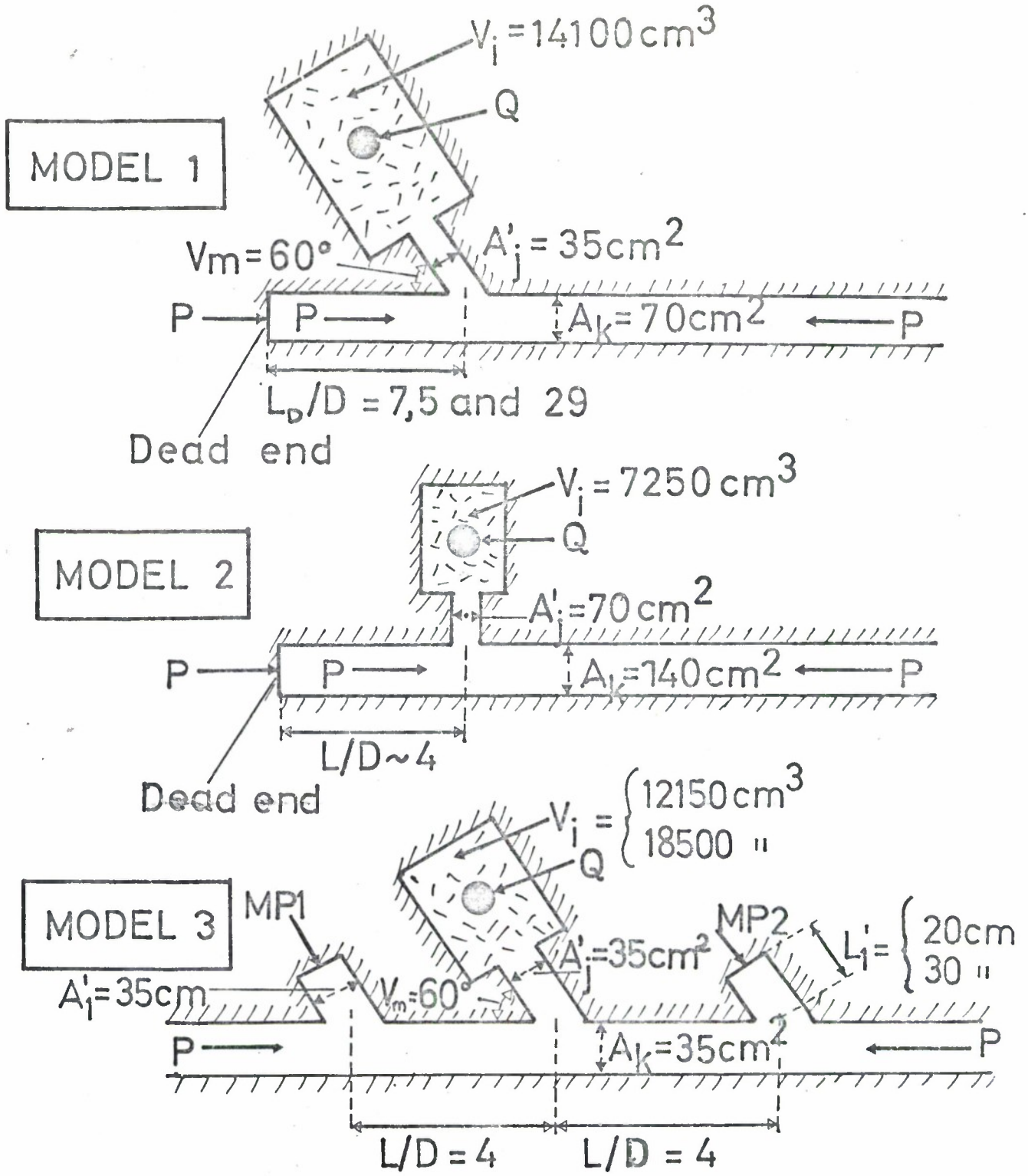

Fig.3.1a. Model configuration of the three sites discussed in Report V.

p denotes pressure measurements.

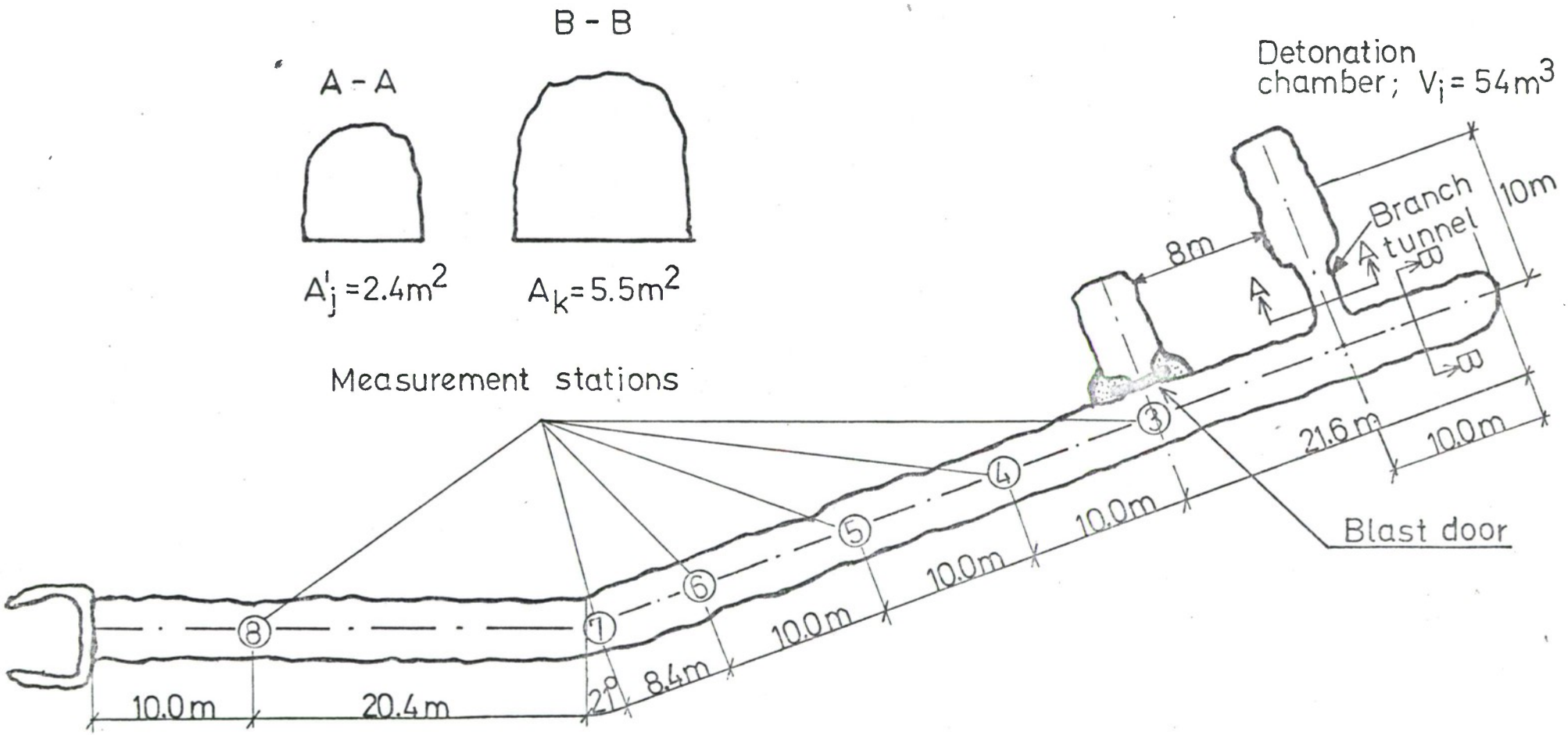

Fig. 3.1b. Tunnel system in the large scale test at Raufoss /8/.

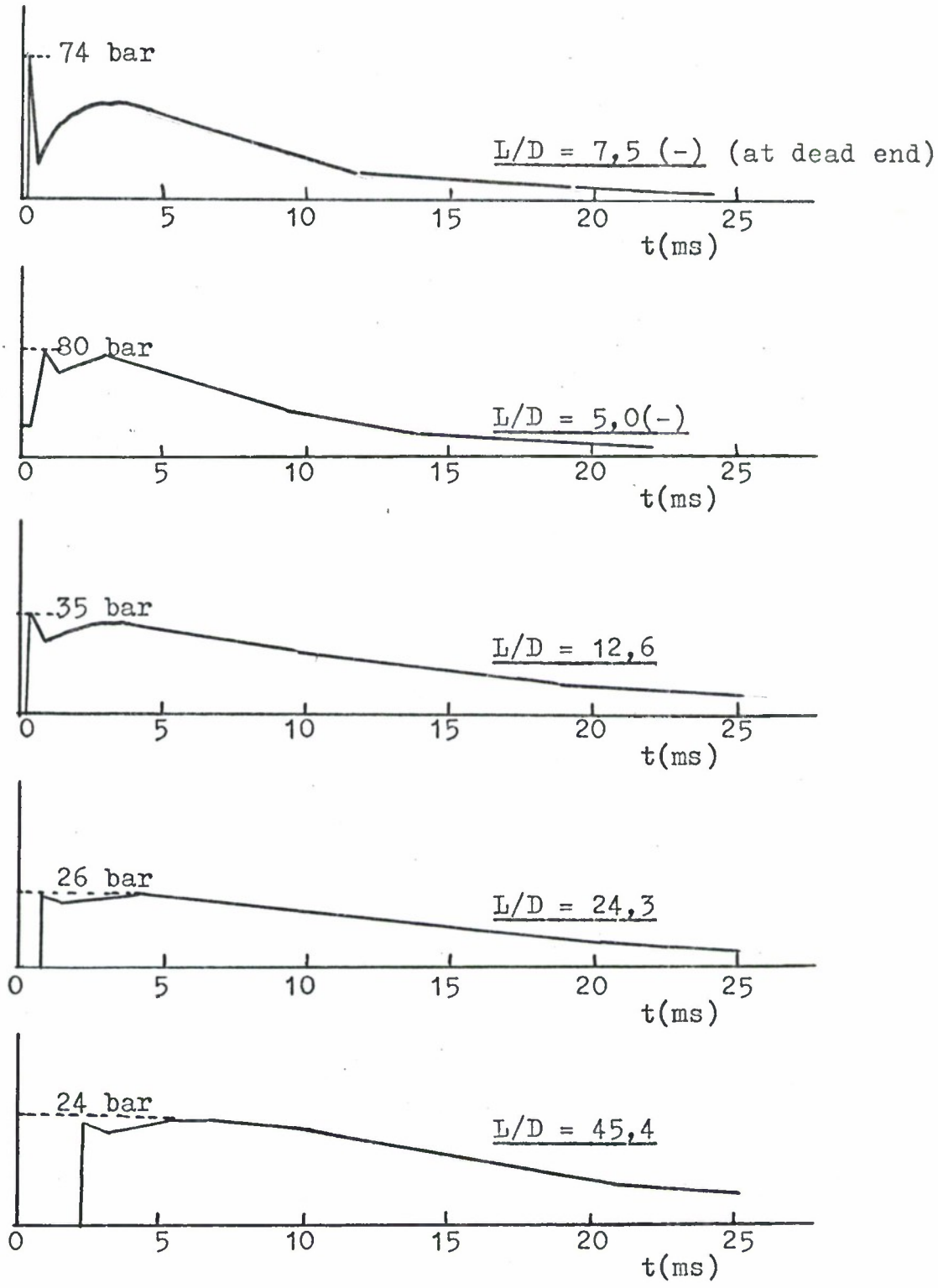

Fig. 4.1a. Averaged pressure-time recordings for Model 1 (Q = 593 g TNT) with L_D/D = 7,5. The minus sign (-) indicates measuring points in the dead end tunnel.

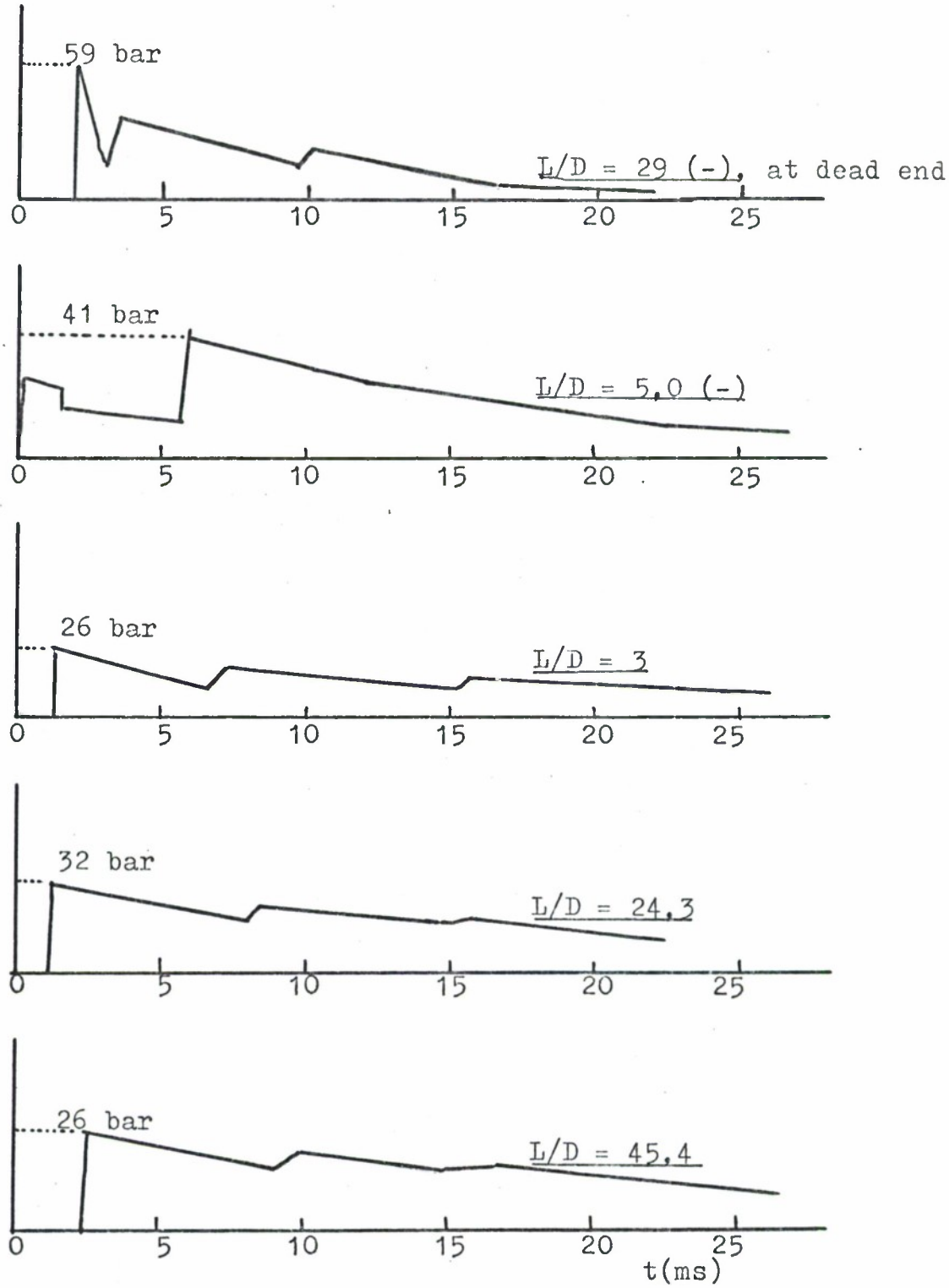

Fig. 4.1b. Averaged pressure-time recordings for Model 1 (Q = 593 g TNT) with L_D/D = 29. The minus sign (-) indicates measuring points in the dead end tunnel.

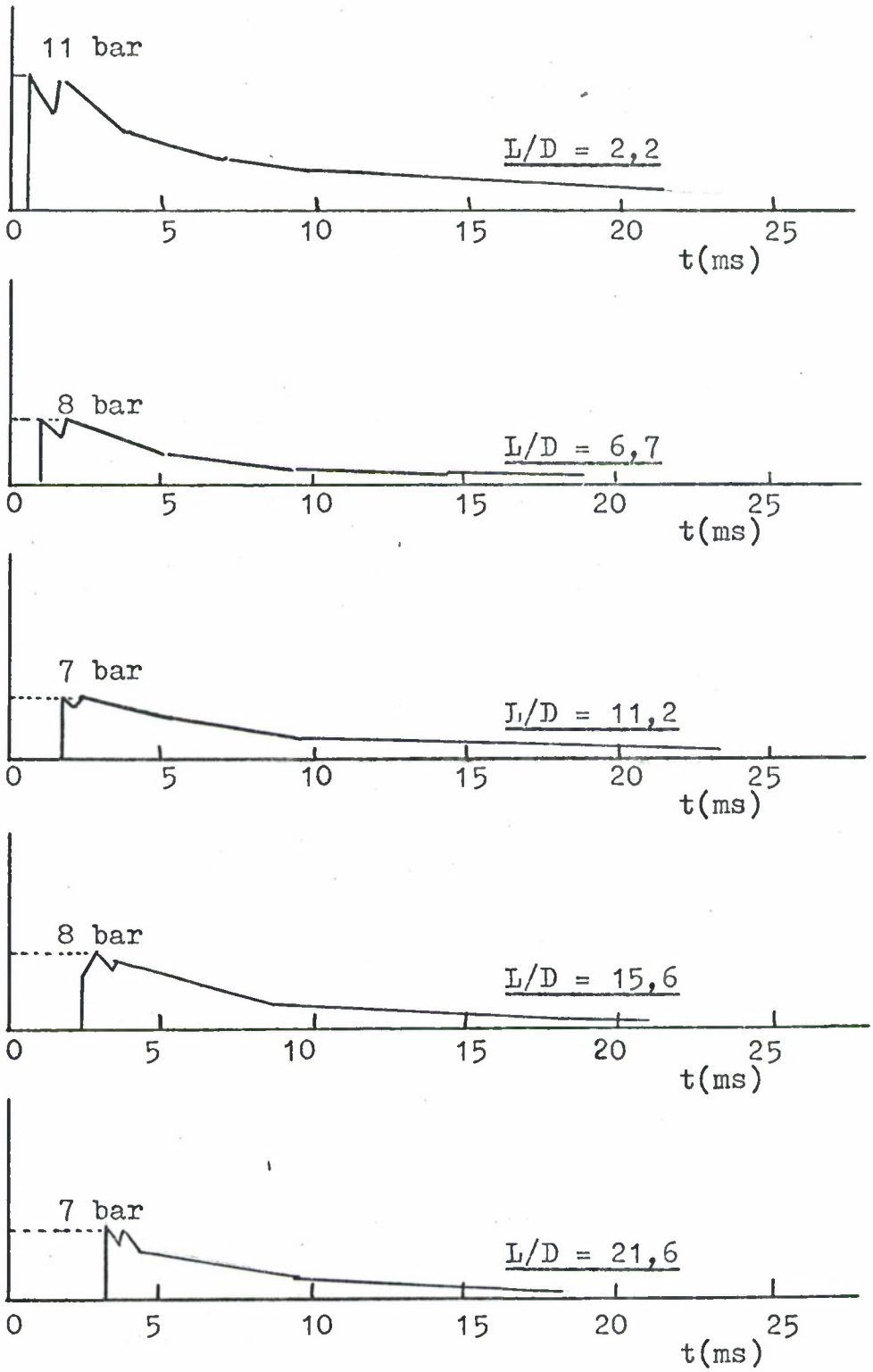

Fig. 4.1c. Averaged pressure-time recordings for Model 2 (Q = 39 g TNT).

$L < L_D$

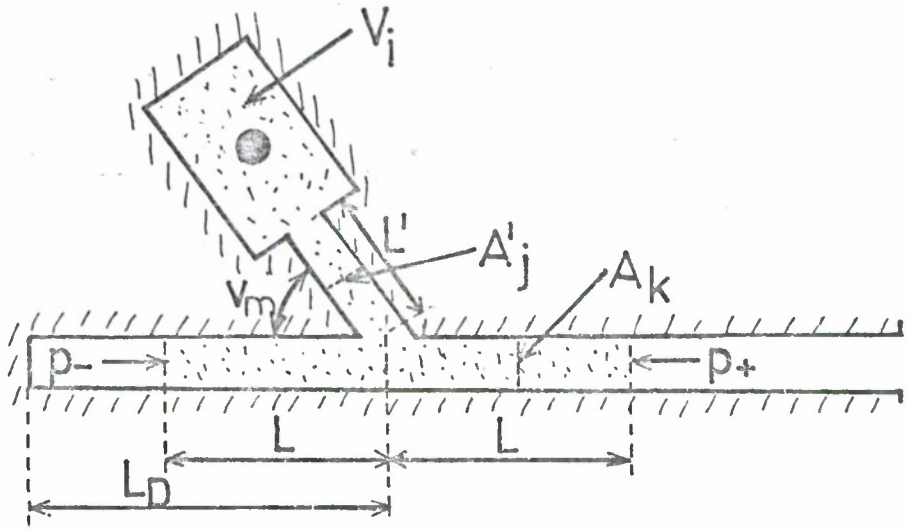

$$\left.\begin{aligned} p_+ &= C_1 (Qx_+ / V_t)^{C_2} \\ p_- &= C_1 (Qx_- / V_t)^{C_2} \end{aligned}\right\} p = C_1 (Qx_\pm / V_t)$$

$$V_t = V_i + A'_j \cdot L' + 2 A_k \cdot L$$

$$x_+ = 2(1 - v_m / 180^\circ)$$

$$x_- = v_m / 90^\circ$$

Fig. 4.1d. Definitions of terms used in the scaling relationship for peak pressure at distances $L < L_D$ where L_D is the length of the dead end tunnel.

$L > L_D$

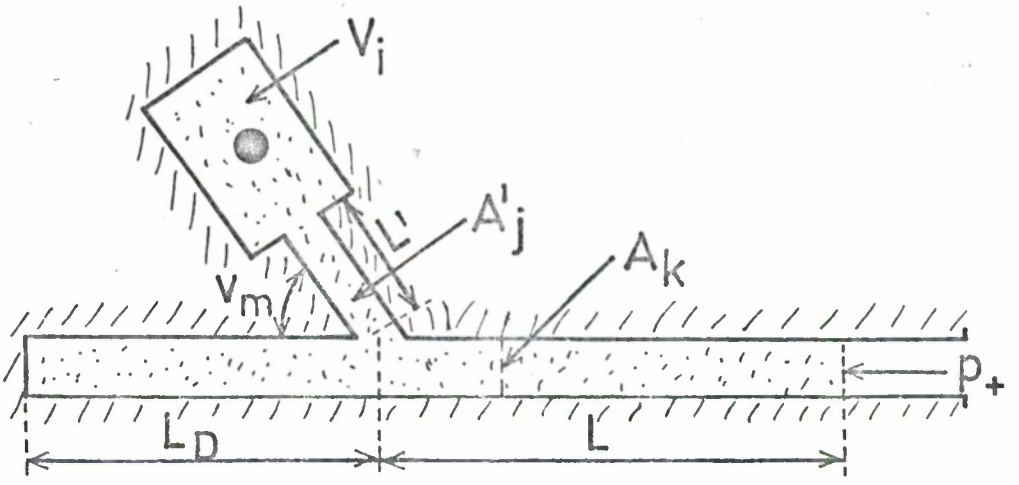

$$p_+ = C_1 (Q X_+ / V_t)^{C_2}$$

$$V_t = V_i + A'_j \cdot L' + A_k \cdot L_D + A_k \cdot L$$

$$X_+ = 2(1 - v_m / 180^\circ)$$

Fig. 4.1e. Definitions og terms used in the scaling relationship for peak pressure at distances L L_D, where L_D is the length of the dead end tunnel.

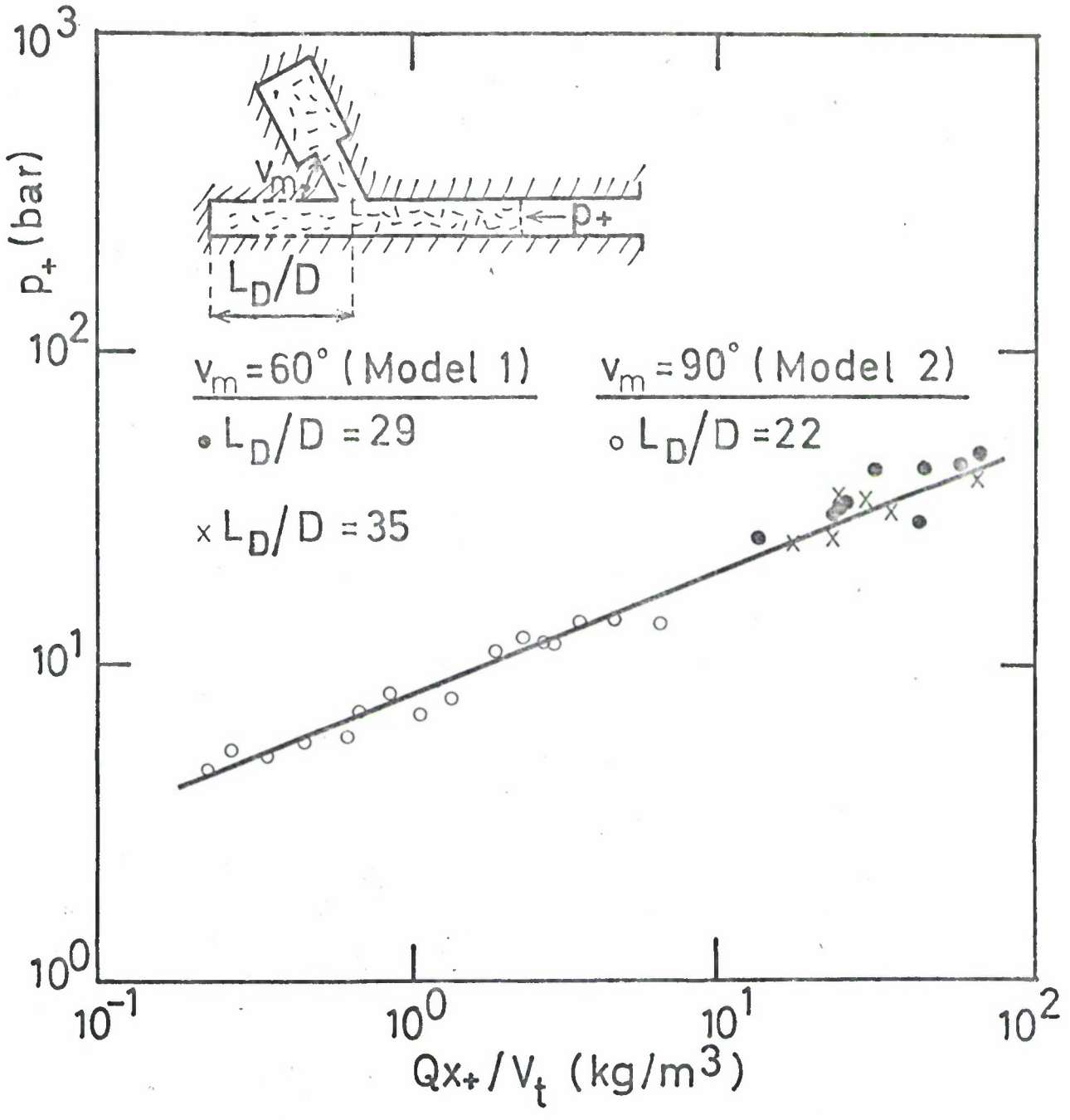

Fig. 4.1f. Peak pressure versus effective loading density for Model 1. See Figs. 4.1a and 4.1b for definition of x_+ and V_t. The solid line represents a least squares fit to all the data.

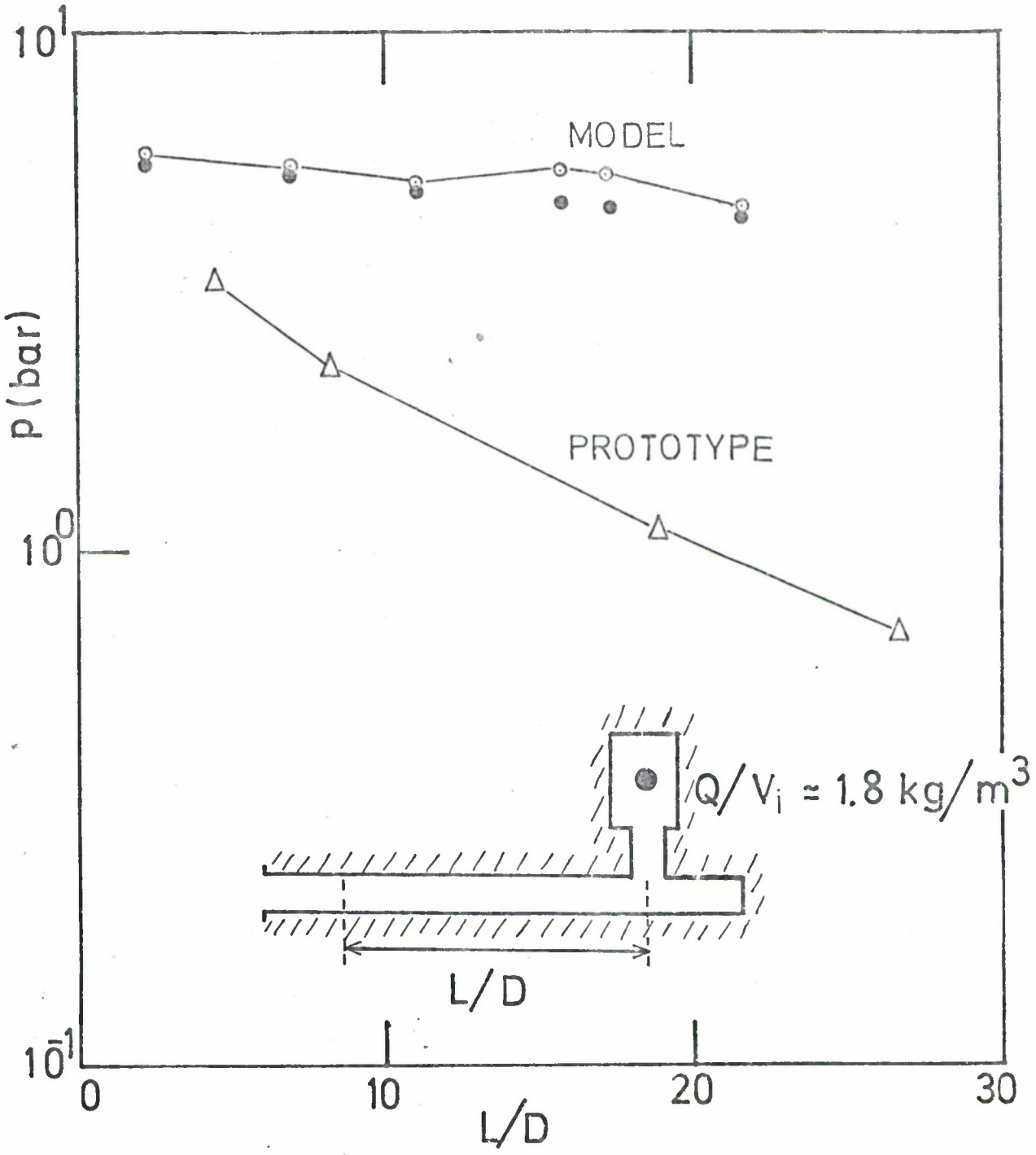

Fig. 4.2a. Peak pressure data compared for Model 2 and prototype. The open and filled circles are the model data deduced from pressure-time recordings and shock-front velocity measurements, respectively.

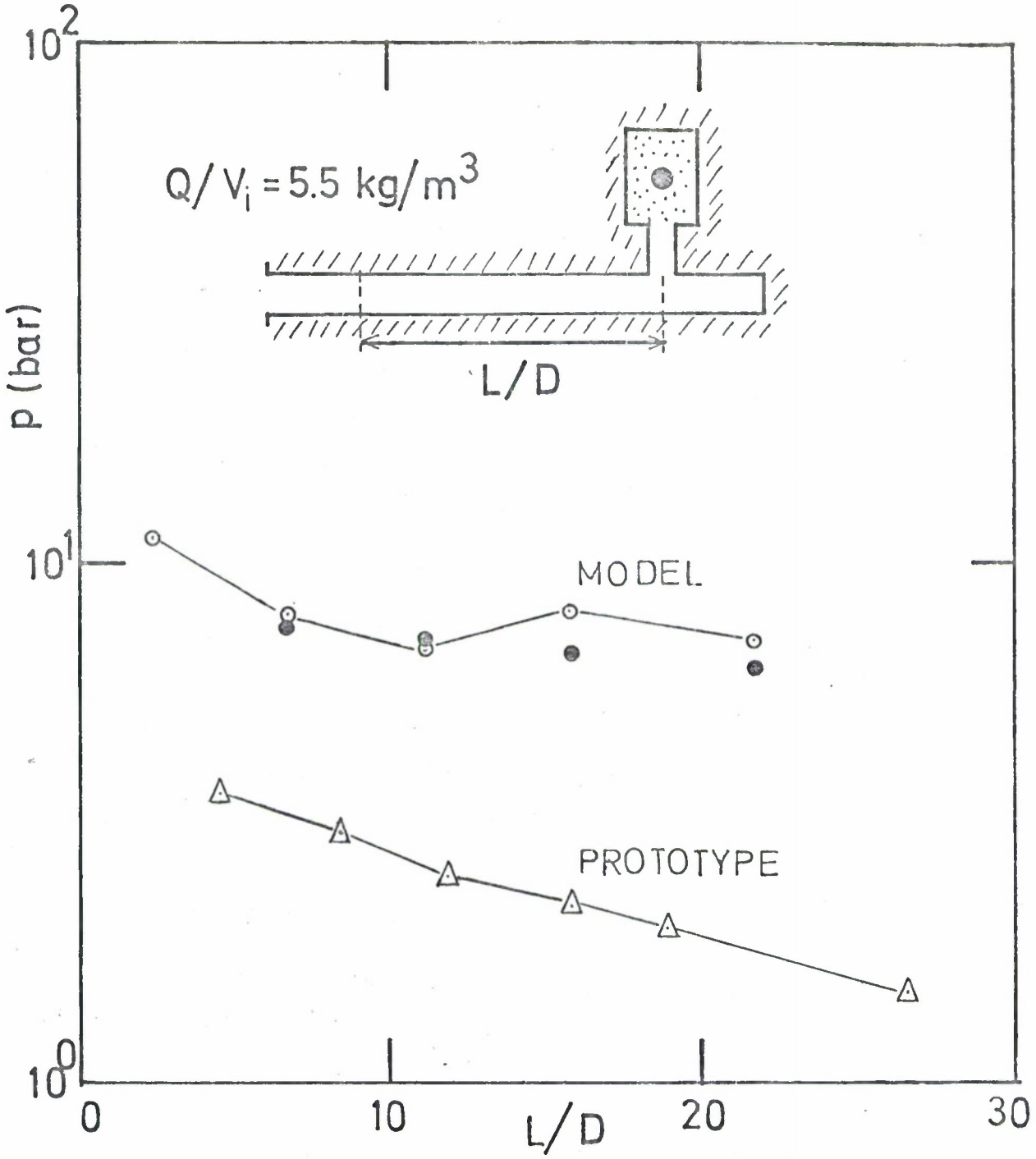

Fig. 4.2b. Comparison of Model 2 and prototype peak pressure data.

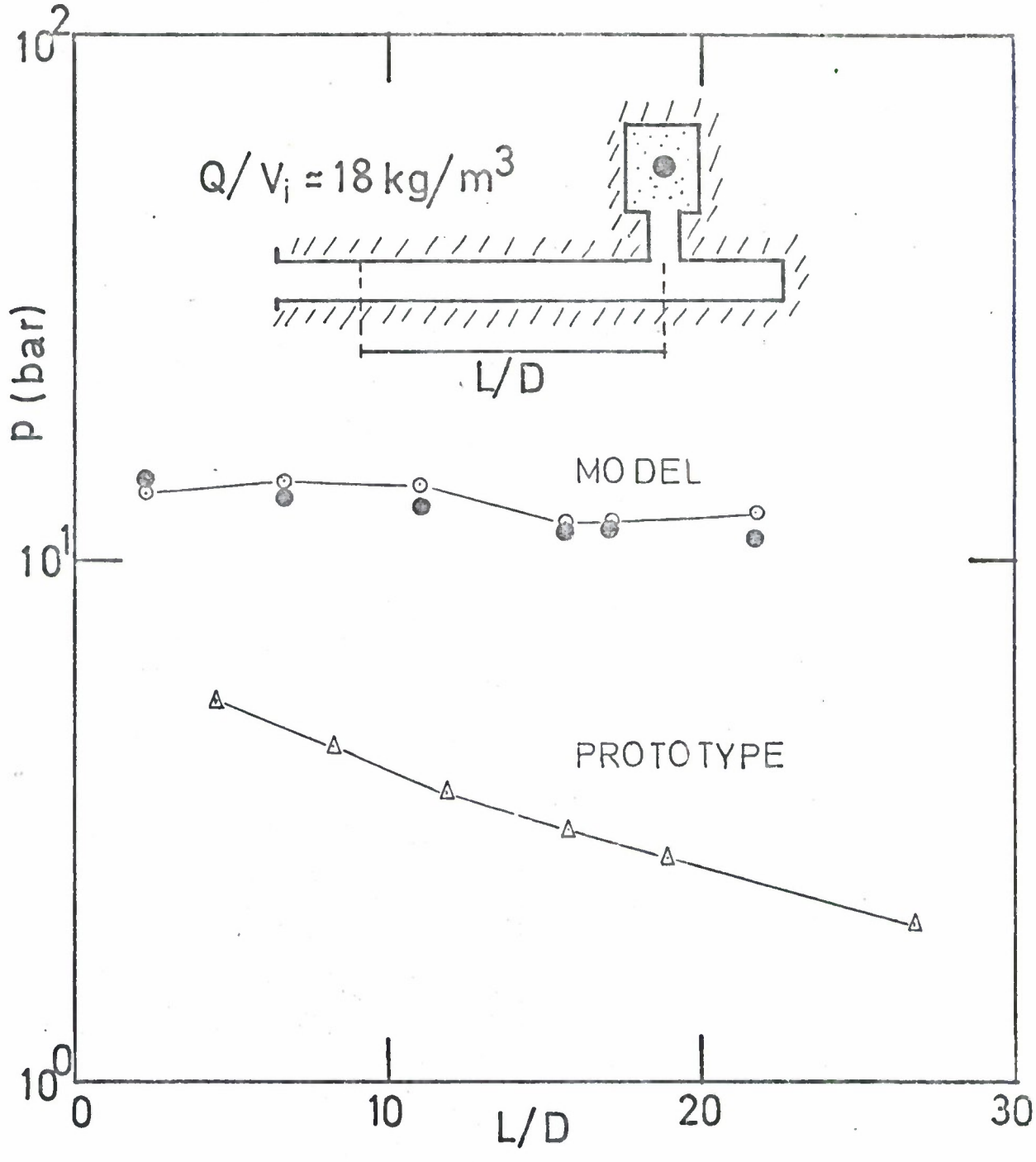

Fig. 4.2c. Comparison of Model 2 and prototype peak pressure data.

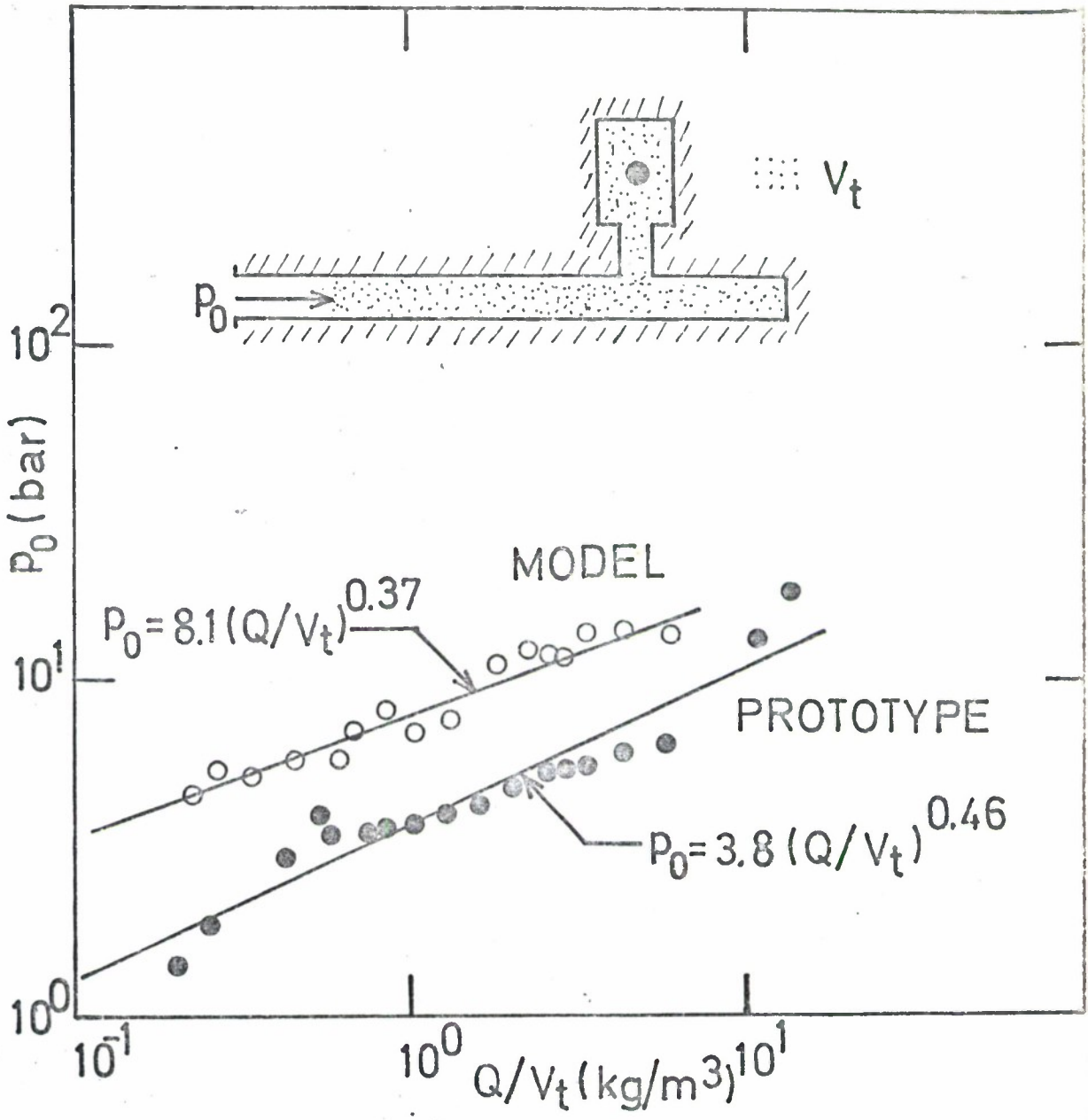

Fig. 4.2d. "Smooth-walled" peak pressure data for prototype compared with model data. The straight lines represent least squares fits to the two sets of data.

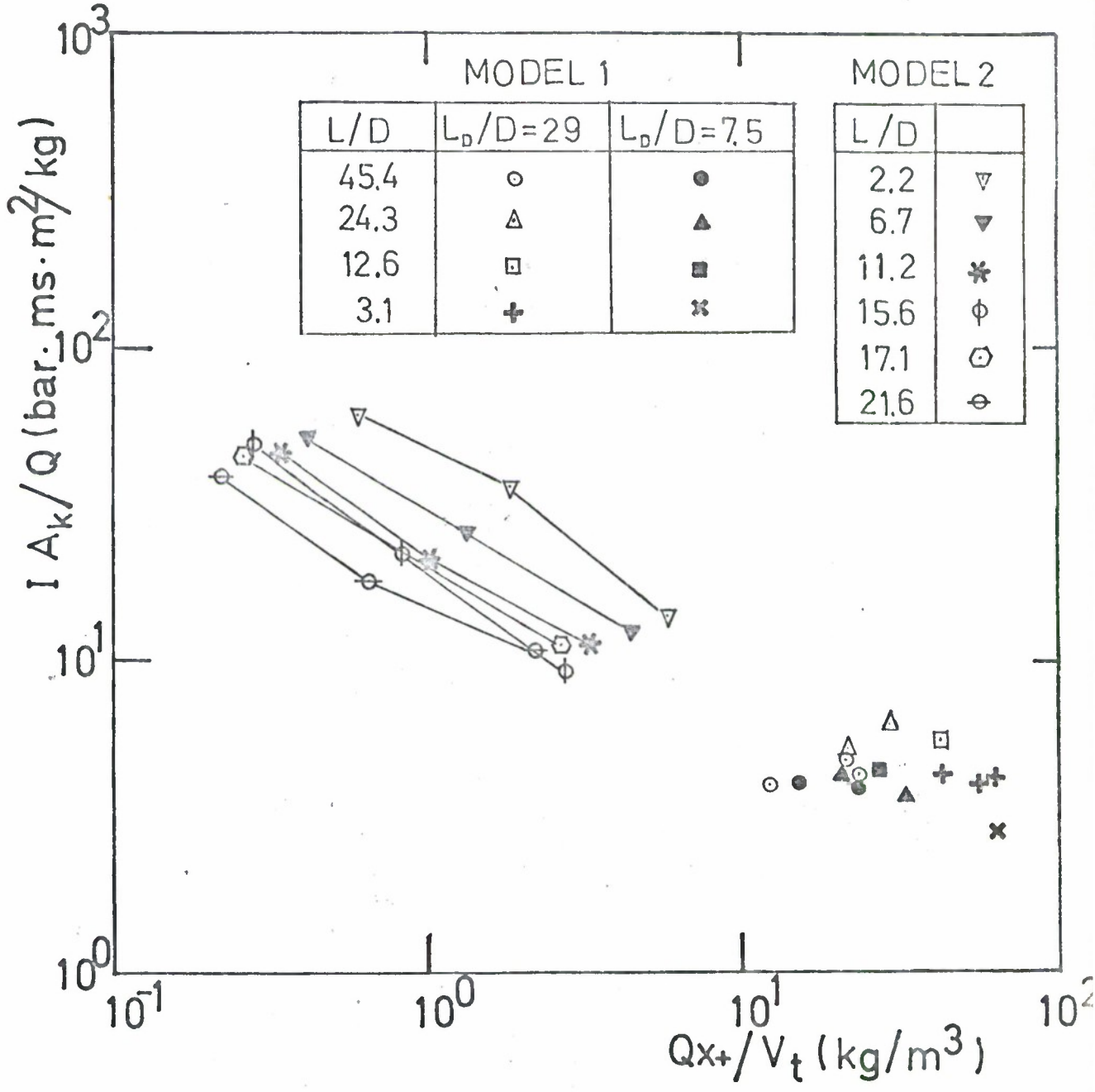

Fig. 4.3a. Scaled impulse data for Model 1 and 2 versus effective loading density.

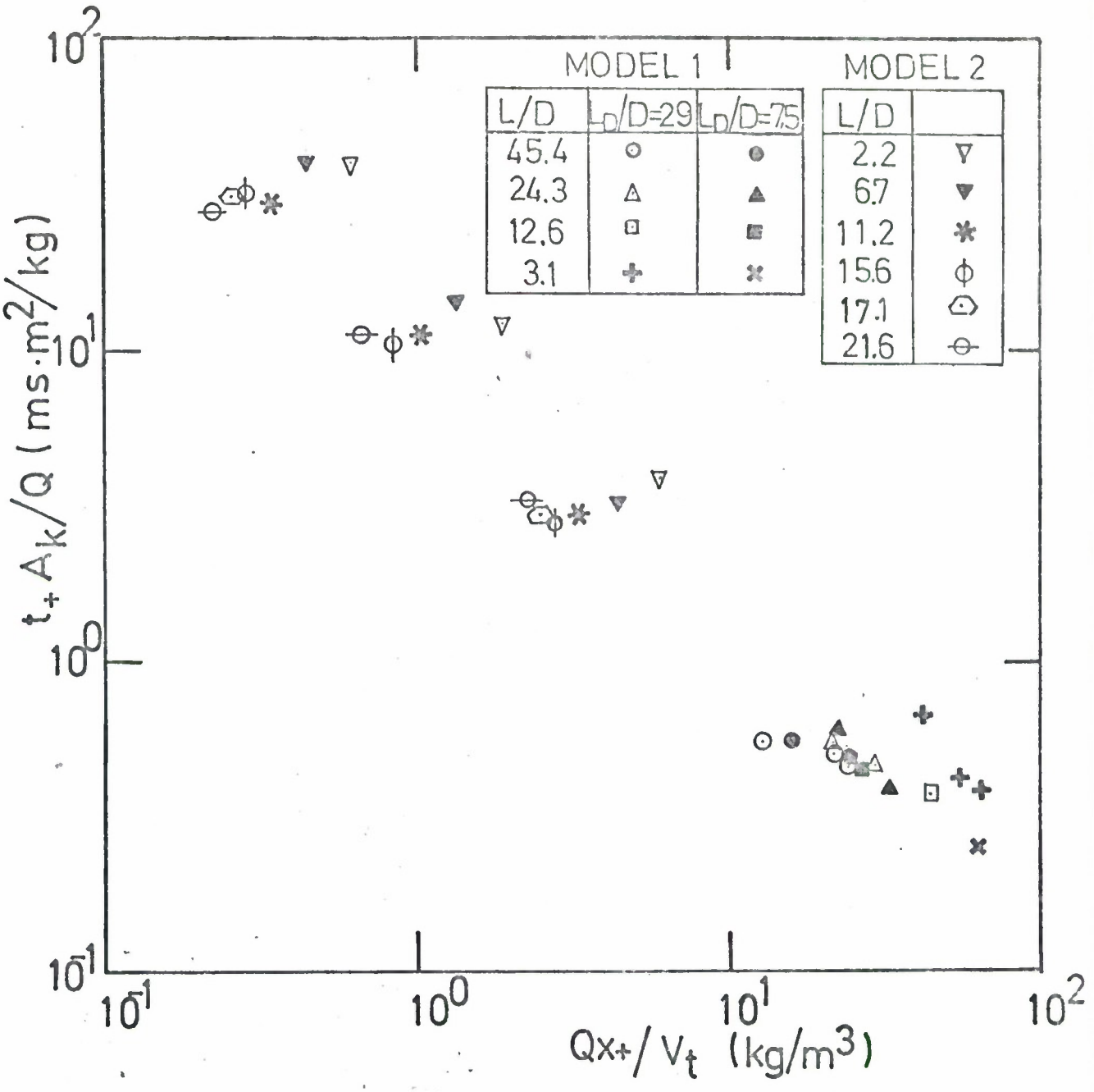

Fig. 4.3b. Scaled positive duration data for Model 1 and 2 versus effective loading density.

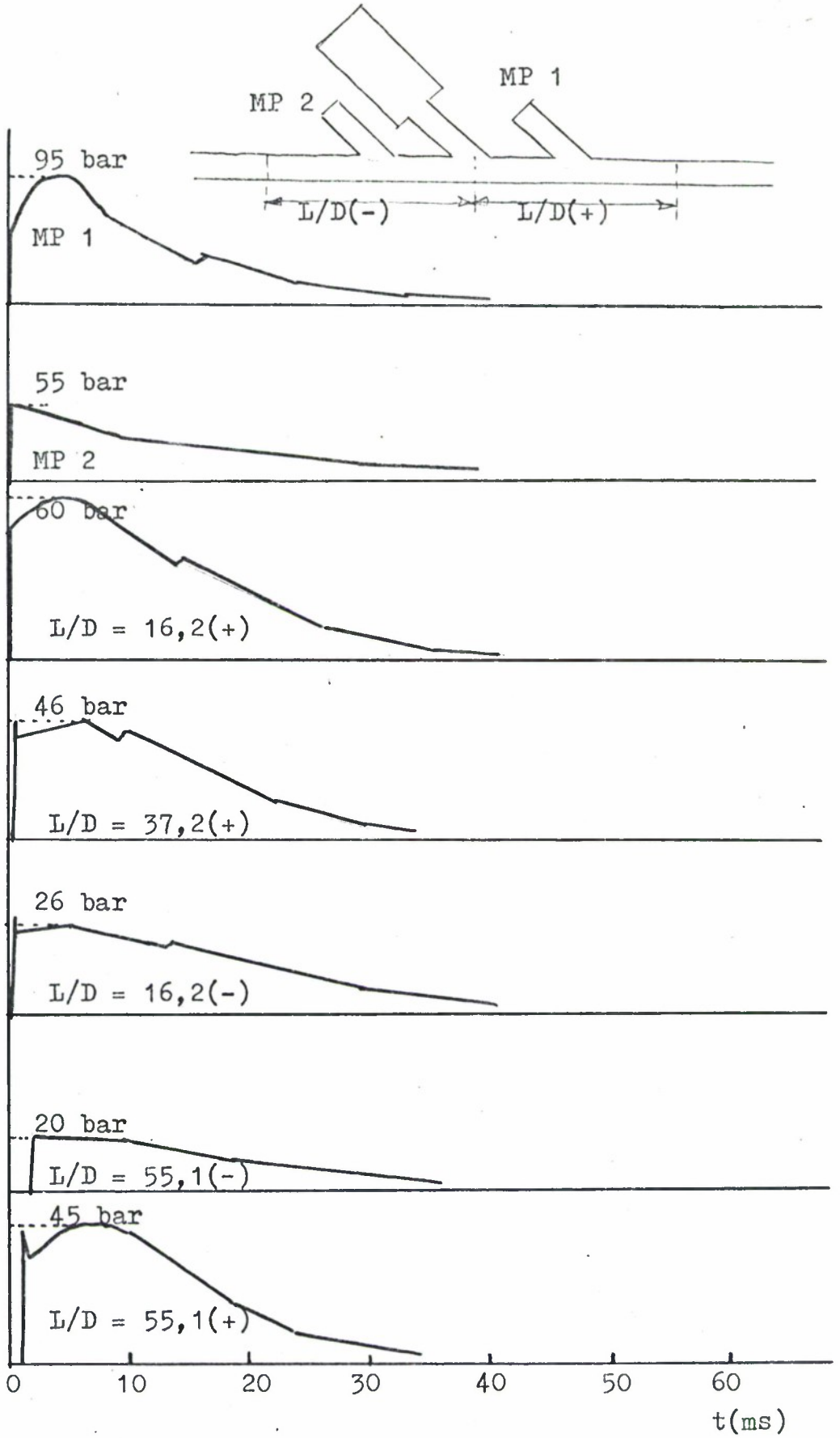

Fig. 4.4a. Averaged pressure-time recordings for Model 3 (Q = 926 g TNT, V_i = 18500 cm^3 and L_1' = 30 cm).

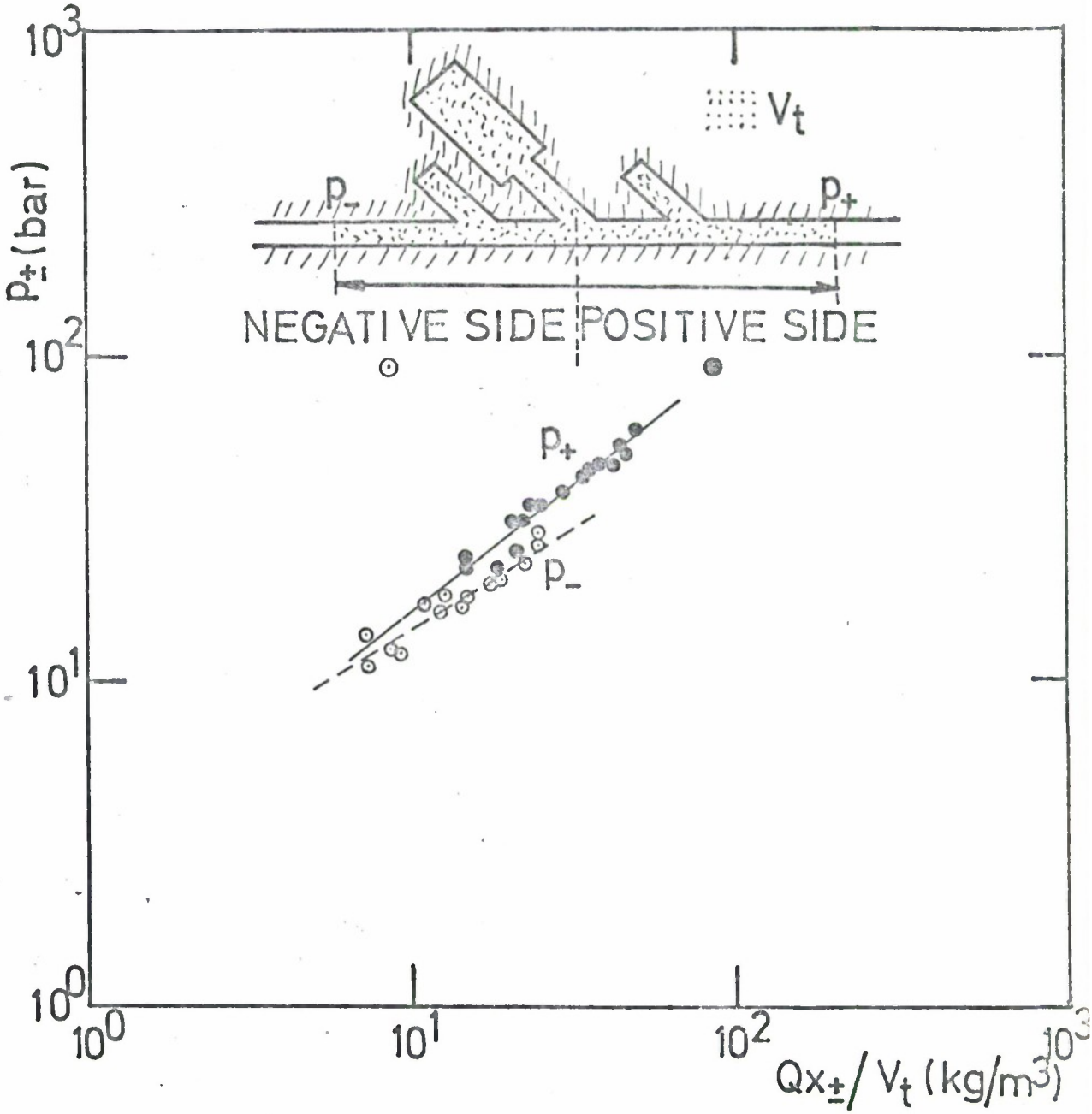

Fig. 4.4b. Peak pressure versus effectiv loading density for Model 3.
The straight lines represent least squares fits to the data as discussed in the text.